Molecular Dynamics Simulation of Aerosol-OT Reverse Micelles

Janamejaya Chowdhary* and Branka M. Ladanyi*

Department of Chemistry, Colorado State University, Fort Collins, Colorado 80523-1872

Received: July 21, 2009; Revised Manuscript Received: August 27, 2009

Molecular dynamics simulations are performed for the reverse micelles (RMs) formed by the surfactant Aerosol-OT (AOT, sodium bis(2-ethylhexyl)sulfosuccinate) in isooctane. The appropriate simulation methodology is identified and applied to the study of the effect of RM size, as quantified by $w_0 = [H_2O]/[AOT]$, on the structure of the reverse micelle. The radial and intrinsic density profiles, pair densities and pair orientations in the first solvation shell, and water−water hydrogen bonding profiles were constructed. On the basis of these various structural characteristics, we find that the organization of sodium ions, sulfonate headgroup, and water oxygen atoms at the surfactant interface is consistent with a pseudolattice structure for $w_0 = 2$. An increase in the RM size leads to the disruption of this lattice, with more sodium ions dissociating from the sulfonate headgroup and an increase in the aqueous solvation of these two species. The water molecules exist primarily in the interior of the RM and exhibit bulklike properties only for $w_0 \sim 7.5$. Some water molecules and sodium ions exist in the intersulfonate headgroup region and interact with the AOT carbonyl group.

I. Introduction

Reverse micelles (RMs) are surfactant aggregates in a nonpolar solvent and frequently contain a nanoscopic polar liquid, typically water,[1−4] in their interior. Due to the different polarity of the interior and nonpolar solvent separated by the surfactant, RMs provide an environment for selective solvation with numerous applications ranging from selective biomolecular solvation with applications in drug delivery,[1,4] controlled biochemical synthesis and catalysis,[5] nanomaterial synthesis,[6] and as model systems with an interior that mimicks cells.[7−9] Numerous experimental studies[10−17] have revealed that water in RMs has properties that differ significantly from that of bulk water,[18] although a molecular level understanding is still a work in progress.

A prototypical surfactant that readily forms RMs is Aerosol-OT (AOT, sodium bis(2-ethylhexyl)sulfosuccinate; Figure 1). It contains a polar sulfonate headgroup and a pair of branched hydrocarbon tails (Figure 1) that give it the ability to solubilize water pools in a nonpolar solvent.[19] The composition of AOT RMs is well described by the parameter $w_0 = [H_2O]/[AOT]$, and the radius of the RM is linear in w_0. Due to the widespread use of AOT, computer simulations of the AOT RMs are important for providing a molecular basis for interpreting experiments. The earliest simulation of an AOT RM in toluene by Alaimo and Kumosinski[20] utilized an all-atom representation for the molecules and addressed the issue of aggregate stability. Faeder and Ladanyi[21−24] studied the size-dependent properties of the RMs' interior using a reduced representation in which the surfactant headgroup was replaced by a single charged interaction site attached to a confining spherical wall and the hydrophobic solvent was replaced by a continuum. All-atom simulations for AOT RM in isooctane were later employed by Abel et al.,[25] although their simulations appear to be unstable at long times, and by Gardner et al.,[26] but they focus on the effect of simulation time and initial configuration on RM structure using molecular compositions that differ from those obtained from experiments. Coarse-grained representations of the surfactant and hexane molecules have also been utilized by Mudzhikova et al.[27,28] in their studies of AOT RMs, by an approach particularly well suited for simulating large RMs.

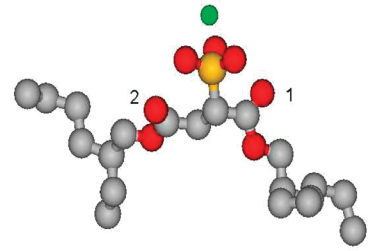

Figure 1. Structure of Aerosol-OT in the united-atom representation for CH_x groups showing (a) sulfur (yellow), (b) oxygen (red), (c) sodium (green), and (d) carbon (gray) atoms. On the basis of the distance from the sulfur atom, the two carbonyl oxygen atoms are labeled 1 (proximal) and 2 (distal).

An important observation from the all-atom and coarse-grained studies of the AOT reverse micelle is that it has an instantaneous quasi-spherical shape that fluctuates with time.[25−27] The same feature has also been noticed in simulation studies of the quasi-spherical RMs formed by the surfactants $C_{12}E_2$,[29] fluorosurfactants,[30] sodium octanoate,[31,32] sodium dodecyl sulfate,[33] and model dichain surfactants.[34,35] Thus, the RM has a quasi-spherical shape that fluctuates about a reference spherical surface primarily due to capillary wave fluctuations.[36,37] Due to the quasi-spherical shape, detailed information on RM structure should be obtained from spherically symmetric radial density profiles complemented with intrinsic density profiles, that is, density profiles constructed with respect to and normal to the instantaneous surface. Previous studies of intrinsic structure for planar liquid/vapor,[38] liquid/liquid interfaces,[39−42] lipid bilayers[43] and reverse micelles[21,44−46] have shown the presence of enhanced density at the interface, and this has important implications for experimental investigation of RM structure.

Experiments provide information on the local environment of different species, and an approximate picture of RM structure can be inferred from this. Since an RM provides an environment

* E-mails: janamejaya.chowdhary@gmail.com; bl@lamar.colostate.edu.

10.1021/jp906915q CCC: $40.75
Published on Web 10/20/2009

suitable for studying the effect of confinement on water, many IR experiments have focused on AOT RM structure and dynamics in terms of the O−H (or O−D) stretching mode of water.[47,48] The broad peak in the spectrum corresponding to the O−H (O−D) stretching mode around 3500 cm $^{-1}$ can be deconvoluted to obtain multiple Gaussian contributions, with each contribution interpreted as a subensemble of water O−H (or O−D) in different local environments. The variation of the fractional contribution of different Gaussian components to the full signal with RM size has been interpreted within the framework of a core−shell model that postulates the existence of a bulklike water core within the RM and a shell region of water molecules coordinated to the surfactant sites. The same model can be used to rationalize experimental results for vibrational energy relaxation, although it is not suitable for interpreting spectral-diffusion and rotational anisotropy due to dynamical exchange between core and shell regions.[12−14] Experimental studies of the RM formed by other surfactants also confirm the existence of a bulklike core.[15]

In the core−shell model, the shell region contains the interface of water with the surfactant. Insight into the arrangement of the headgroup and counterions at this interface can be inferred from, for example, the IR study of symmetric and asymmetric sulfonate stretches[49−54] and ^{23} Na NMR experiments.[55,56] These studies suggest the presence of water molecules bridging pairs of sulfonate oxygen and sodium ions[54] and an increase in dissociation of $^{23}Na^+$ from the headgroup as the RM size increases. Combined with calorimetric data,[57] it appears that the headgroup and counterion exist in a quasi-lattice arrangement, particularly in small RMs, and this lattice structure is broken in the larger RMs. The nature of this pseudolattice is not exactly known, but for the limiting case of waterless AOT RMs, Monte Carlo simulations indicate the presence of a polyhedral shell arrangement.[58]

In this work, our objective is to present our initial results for the structure of AOT RMs on the basis of analysis of configurations obtained from molecular dynamics simulation trajectories. This work complements previous studies of a reduced model for the RM interior by Faeder and Ladanyi,[21] which was geared toward a molecular interpretation of water pool properties. This manuscript is organized as follows: In Section II, we present details of the setup of the system and force fields used for the simulation, stability of the RM, and details of the numerical implementation of the intrinsic structure calculation. The radial and intrinsic profiles for various structural characteristics are presented in Section III. Information on the overall distribution of molecular species in the RM interior is then supplemented with pair distribution functions in Section IV and pair orientation in the first coordination shell in Section V. Next, we present our results for the water−water hydrogen bond network in Section VI and conclude with a summary and brief discussion of our results in Section VII.

II. Simulation Details

A. Molecular Dynamics. In this section, we present a detailed description of the different components of our molecular dynamics (MD) simulations of the RM aggregate formed by the surfactant AOT in isooctane (2,2,4-trimethyl pentane). We start by presenting the interaction models employed in the simulation. Water was modeled with the rigid nonpolarizable three-site SPC/E model[59] that includes charges on all sites and a Lennard-Jones interaction site on the oxygen atom. The interaction parameters for Na^+ were taken from Schweighofer et al.[60] A united-atom representation in which the methylene and methyl groups are represented by a single interaction site was adopted for the AOT molecule. All internal degrees of freedom are included except for bond lengths, which are kept fixed. The molecular geometry and interaction parameters were taken from the TraPPe force field.[61,62] Since the TraPPe force field does not contain parameters for the sulfonate headgroup, we use the CHARMM lipid force-field parameters and charges[63] for its sulfur and oxygen atoms and for the headgroup internal degrees of freedom. Isooctane was used as the hydrophobic solvent, and its interactions were modeled with the TraPPe force field for branched hydrocarbons.[61] As with the CHARMM force field, all intramolecular nonbonded interactions between sites separated by four or more bonds are treated as the Lennard-Jones interaction, in which the parameters were obtained using the Lorentz−Berthelot mixing rule but the energy scale was halved. All force field parameters have been summarized in the Supporting Information.

In molecular simulations, Lennard-Jones interactions between pairs of sites are typically truncated at some radial distance, R_c. The effect of this truncation on thermodynamic properties such as pressure and potential energy is accounted for by including correction terms that include interactions beyond R_c. The calculation of these correction terms implicitly assumes the pair distribution function, $g(r) \rightarrow 1$, at large radial distances (r). For a pair of molecules inside the RM, such as water and the sodium ion, the pair distribution function $g(r)$ is expected to vanish for $r > d$ where d is the diameter of the RM. For small RMs, this scenario corresponds to $g(r) \rightarrow 0$ for large r. Clearly, the usual corrections to pressure and potential energy are inapplicable for such pairs of molecular sites. In this scenario, the long-range correction for an instantaneous configuration can be calculated on the basis of the actual radial distribution function corresponding to $r \geq R_c$ for each pair of interaction sites. Here, we use the much simpler approach of considering the full interaction between molecular sites of water and AOT. Interactions of water and AOT with the solvent are truncated at $R_c = 15$ Å, and the normal energy and pressure corrections are applied, since for these interactions, the approximation $g(r) \sim 1$ for $r > R_c$ is reasonable due to the expectation of bulk densities at large r for the solvent.

Ewald summation[64,65] was employed to handle electrostatic interactions using a real space cutoff of $L/2$, where L is the length of the simulation box (defined in the next paragraph). For the reciprocal space contribution, we use a damping parameter, $\alpha = 5.6/L$; a maximum value of $10\pi/L$ for each component; and a maximum magnitude of $20(3)^{1/2}\pi/L$ for the reciprocal space wave vector. The mechanical expression for the pressure tensor was used, since the system volume is large enough, and consequently, the thermodynamic definition is not essential.[66]

Molecular dynamics simulations are performed using the velocity-Verlet[65] algorithm at 1 atm and 298.15 K using a time step of 0.002 ps. The pressure and temperature were maintained using Berendsen's method[67] with the bath coupling time of 1 ps for the thermostat as well as for the barostat. For molecules involving rigid intramolecular degrees of freedom, we use RATTLE[65] to constrain the bond lengths and angles. All simulations of the RM system were performed in a truncated octahedral box, and periodic boundary conditions appropriate to this simulation box were employed. This choice of the simulation box minimizes the number of hydrocarbon molecules required for solvating the RM. It also minimizes the corner effects associated with a cubic box.[65] Since a truncated octahedral simulation box can be obtained by cutting off the

TABLE 1: Reverse Micelle Size, Composition, and Simulation Times[a]

run	w_0	n_s	n_w	n_{hc}	t_e	t_d	t_s	R_s
RM2	2	26	52	187	5.0	1.0	6.0	8.3
RM4a	4	35	140	527	5.0	1.0	6.0	10.6
RM4b	4	35	140	522	5.0	1.0	6.0	10.9
RM5.1	5.1	42	211	817	4.5	0.5	5.0	12.1
RM7.5	7.5	70	525	1403	2.5	0.2	2.7	16.2

[a] n_s, n_w, and n_{hc} are the number of surfactant, water, and isooctane molecules, respectively. The equilibration, data collection, and total simulation times, t_e, t_d, and t_s are reported in units of nanoseconds. The size of the RM (R_s), as quantified by the average distance of the sulfur atom from the RM center of mass, is reported in units of Angstroms.

corners of a cubic box, we identify the box length L with the edge of the untruncated cubic box.

The composition of the RM system can be specified in terms of the number of water (n_w), surfactant (n_s) and hydrocarbon solvent molecules (n_{hc}). The number of molecules of each component of the RM is selected from ref 21 and listed in Table 1 for convenience. These parameters were derived from the light-scattering experiments of Eicke and Rehak[68] and differ from the compositions obtained from small-angle X-ray scattering experiments of Amararene[69] that were used by Abel et al.[25] in their simulations of the AOT RM. For a given w_0, the stability of the RM depends on the selected composition, and we expect some differences between our results and those of Abel et al.[25]

For constructing each RM, we start with an MD simulation of 1000 water molecules in a cubic box at 1 atm and 298.15 K. A total of $n_s + n_w$ water molecules were selected from the cubic box in the order of proximity to the center of mass of the simulation box. This ensures a roughly spherical water phase. Of the selected water molecules, n_s, of the outermost molecules are selected at random and replaced with a single site corresponding to Na^+ such that the center of mass of the water molecule now corresponds to the position of Na^+. The maximum radial distance (R_1) of any site in the water/Na^+ configuration from the origin is estimated, and a sphere of radius $R_1 + \sigma_1$ is constructed, where σ_1 is twice the LJ interaction parameter for AOT sulfur/water oxygen interactions. Sulfur atoms are placed on this sphere, one at a time, and the interaction energy of these S atoms is minimized. For this purpose, the LJ σ parameter for the sulfur atom is doubled and varied within 5%σ to generate maximally separated pairs of sulfur atoms on the sphere.

The AOT molecule is reconstructed around each S atom such that the vector from the sulfur atom to the center of mass of the AOT molecule is aligned with the vector from the origin of the sphere to the sulfur atom. A positive charge with magnitude $-n_s$ is placed at the origin of the sphere to attract the charged sites on the AOT molecule inward. The interaction of the charged sites on AOT with the spherical shell is treated with the repulsive part of the LJ pair potential with the σ parameter equal to that of the oxygen site on water and the ε parameter obtained using the Lorentz−Berthelot mixing rule[65] for the oxygen site on water and charged sites on AOT. The AOT molecules are then allowed to interact with each other, with the shell, and with the interior static charge. This step is followed by MD simulation of the cluster at 298.15 K for 250 ps to equilibrate the AOT molecules. The equilibrated water/sodium cluster is then placed inside the spherical cavity formed by the AOT molecules, and the system is equilibrated for another 250 ps at 298.15 K. To prevent the water molecules inside the aggregate from diffusing outside, we introduce an infinitely thin shell around the water pool at a radius corresponding to the RM radius. The interaction of this shell with water oxygen was modeled as the repulsive core of the LJ pair potential with the parameters for the water oxygen. This shell interacts with the water molecules only and allows the ions as well as the surfactant headgroups to equilibrate in water.

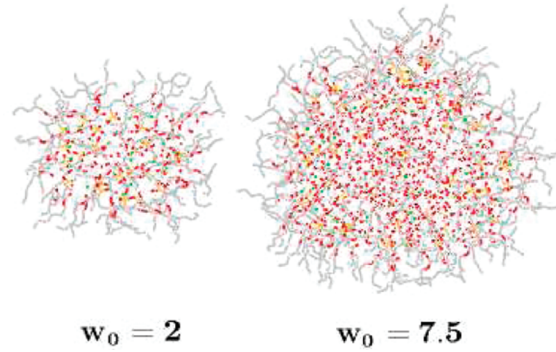

Figure 2. Representative equilibrium reverse micelle configurations for RM2 and RM7.5 containing (a) water (red oxygen atom, white hydrogen atom), (b) sodium (green), (c) AOT (S (green), O (red), and hydrocarbon tail (gray)).

Next, we determine the radius of the smallest spherical cavity (R_2) containing all the molecules in the equilibrated configuration obtained in the last step. An MD simulation of isooctane in a truncated octahedral box is performed such that the box length is at least $R_2 + R_c/2$. This ensures that the number of hydrocarbon molecules needed for the simulation is minimal and also ensures that interactions between AOT hydrophobic tails are absent. The hydrocarbon solvent is equilibrated for 250 ps, and the water/AOT aggregate is transferred to the center of the hydrocarbon box. All hydrocarbon molecules that overlap with the RM aggregate are deleted. The resultant configuration is equilibrated using MD simulation for time t_e (listed in Table 1), after which configurations are saved every 2 time steps up to time t_d (Table 1) for analysis. Sample configurations for the $w_0 = 2$ and 7.5 RMs obtained after time t_e are shown in Figure 2 to illustrate the shape of the RM obtained from our simulations. Slight changes in RM composition such as for RM4a and RM4b do not affect the RM structure significantly, and we present data for RM4a wherever we refer to the $w_0 = 4$ RM in the following unless explicitly specified.

B. Reverse Micelle Stability. *1. Size.* A primary concern in the simulation of an RM is its stability. Physically, a stable RM is expected to confine water inside the surfactant layer, have some equilibrium size and shape, and exhibit well-behaved fluctuations about the equilibrium topology. From visual inspection of the configurations obtained from our simulations, we do not observe any water molecules, sodium, and surfactant ions escaping from the confining region and diffusing into the hydrocarbon phase. The simulated RM therefore appears to be a stable aggregate over the simulation timescale.

Further characterization of RM stability requires quantifying its size. As apparent from Figure 2, the RM has a shape that resembles a sphere. An approximate measure of RM size is the average distance, R_s, of the surfactant sulfur atom from the center of mass of the RM. The time variation of R_s is presented in Figure 3a for all RMs simulated in this work. Fitting $R_s(t)$ to a straight line leads to a negligibly small value for the slope of the line, and this indicates the absence of any drift in $R_s(t)$. The RM clearly has a well-defined mean size. The mean radius, $\langle R_s(t) \rangle$, is presented in Table 1. The variance of $R_s(t)$ is on the

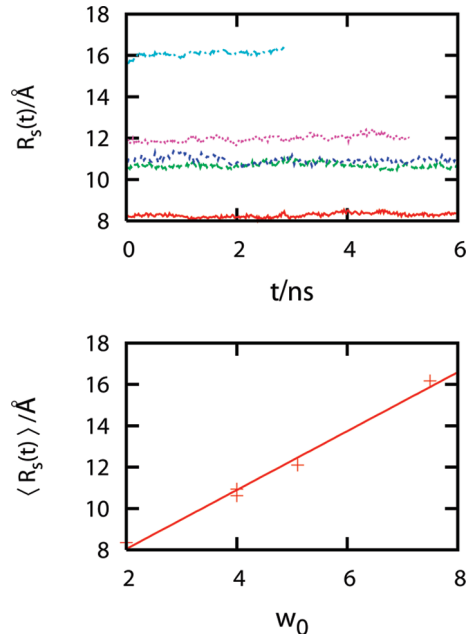

Figure 3. Time variation of the mean radial distance between the sulfur atom and the center of mass of the RM, R_s/Å, over the simulation time of t_s/ns for the reverse micellar systems RM2, RM4a, RM4b, RM5.1, and RM7.5 (bottom to top) at $t = 1.0$ ns.

order of 0.008 Å^2, which is small with respect to $\langle R_s(t) \rangle$. The RM clearly exhibits well-behaved fluctuations about the mean size, as quantified by R_s.

Experimental measurements of the RM size reveal a linear dependence of the water pool radius on w_0.[70,71] Identifying $\langle R_s(t) \rangle$ with the radius of the RM, we plot its magnitude as a function of w_0 in Figure 3b for all simulated RMs. It is clear from this plot that $\langle R_s(t) \rangle$ exhibits a linear increase with w_0, and this is consistent with experiments.

2. Shape. The RM has an overall quasi-spherical shape. The time-varying shape of the RM can be quantified using two commonly employed approaches that utilize the three principal moments of inertia of the aggregate. In the first approach,[34,72] the three principal moments of inertia are calculated for a suitable set of molecules forming the RM. The ratios

$$\eta_1 = 1 - I_{min}/I_{avg} \quad (1)$$

$$\eta_2 = I_{max}/I_{min} \quad (2)$$

where I_{min}, I_{max}, and I_{avg} are the minimum, maximum, and average magnitude of the eigenvalues of the inertia tensor, are then estimated. For a perfect sphere, $\eta_1 = 0$ and $\eta_2 = 1$. Deviations from these reference values indicate the extent of deviation from spherical shape. Alternatively, the principal moments of inertia can be used to replace the aggregate with an equivalent ellipsoid having the same mass and moments of inertia.[25]

We select the first quantification of aggregate shape and present the time series for the two shape parameters, η_1 and η_2, for the entire RM aggregate in Figure 4 for RM2.0 and RM5.1. The shape parameter η_2 corresponds to the asymmetry in the maximum and minimum moments of inertia and fluctuates around 1.28 and 1.19 for $w_0 = 2$ and $w_0 = 5.1$. Since these values of η_2 are close to unity, the shape asymmetry is not significant, a result supported by the small magnitude of η_1 that fluctuates about an equilibrium value of 0.136 and 0.11 for RM2 and RM5.1. At times beyond 3.0 ns, we find both η_1 and η_2 reach values which are almost independent of RM size.

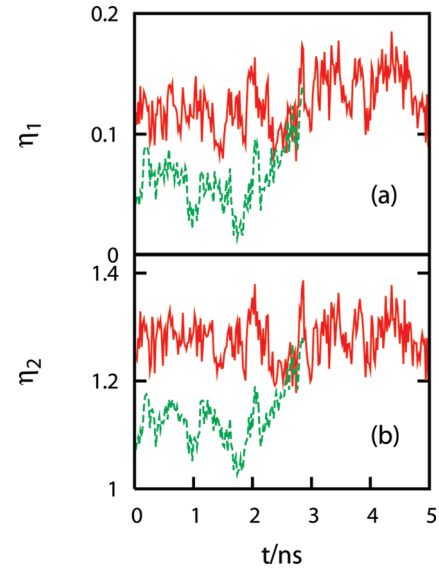

Figure 4. Time variation of the shape parameters (a) η_1 and (b) η_2 for the reverse micelles RM2 (top) and RM5.1 (bottom) over the simulation time of t_s/ns.

C. Constructing the Intrinsic Property. The intrinsic profile for a selected structural characteristic corresponds to its variation with respect to and orthogonal to the local surface. The RM can be thought of as being composed of (a) water/surfactant headgroup and (b) surfactant tail/hydrocarbon interfaces. Instead of using these two interfaces, we select the position of the AOT S atom to represent the intrinsic surface because this is computationally simpler and also because the interfacial configuration of the two interfaces in the RM are dependent on the position of the S atom. Given the quasi-spherical surface formed by the S atoms, the smooth, intrinsic surface passing through these sites is approximated as being locally spherical around each site.[44,46] Due to this local symmetry, the density profile for the locally spherical sections constructed with respect to the surface are normal to the surface. This approximation is reasonable when the overall shape is quasi-spherical and for a large number of surface sites.

Denoting the mean radial distance of all S sites in a given RM configuration by r_m, all S sites are projected radially onto a reference spherical surface with radius r_m. A Voronoi tesselation of this spherical surface generates polygons about each S site, i, whose edges define the range of solid angles, Ω_i (subtended at the origin), for which a point on the surface maps to the surface site i, that is, the catchment basin of each surface site. Next, we project each nonsurface molecular site, j, at a radial distance, r_j (from the origin), onto the reference sphere and map it to the nearest surface site i, which is at a radial distance r_i from the origin. The distance in the radial direction between the intrinsic surface and the molecular site is $d_{ij} = r_j - r_i$. For sites inside the intrinsic surface, $d_{ij} < 0$, whereas for sites outside the intrinsic surface, $d_{ij} > 0$. The intrinsic density profile is calculated from

$$\rho_I(d) = \left\langle \sum_i \sum_{j \to i} \frac{m_j \, \delta(d - d_{ij})}{\Omega_i (r_i + d_{ij})^2 \Delta d} \right\rangle \quad (3)$$

where $j \to i$ indicates a sum over all molecular sites, j, that map to the S site, i; Δd is the width of the shell; m_j is the mass of molecular site j; and the area of the spherical section at a distance d_{ij} from the surface and subtending the solid angle Ω_i at the origin is $\Omega_i (r_i + d_{ij})^2$. Similar to the intrinsic density

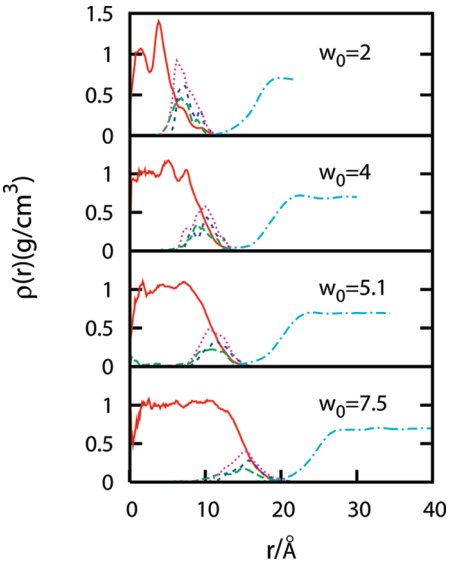

Figure 5. Radial density profiles for the water oxygen atom (solid/red line), sodium ion (large dashes/green), headgroup sulfur atom (small dashes/blue), headgroup oxygen atom (dots/pink), and 2,2,4-trimethyl pentane (large dash-dot-large dash/teal) in different sized reverse micelles.

profile, the intrinsic profile for any structural characteristic, X_j, of molecular site j can be constructed from

$$\rho_{X,I}(d) = \left\langle \frac{\sum_i \sum_{j \to i} X_j \, \delta(d - d_{ij})}{\sum_i \sum_{j \to i} \delta(d - d_{ij})} \right\rangle \quad (4)$$

III. Spatial Organization of the System

A. Radial Density Profile. Here, we present the spherically symmetric radial density profiles constructed with the origin at the instantaneous center of mass of the RM. Since the position of the origin fluctuates with time, does not coincide with the actual position of a molecular site, and has a vanishingly small volume, averaging at the origin will be poor. Furthermore, the quasi-spherical shape and fluctuations of the instantaneous RM shape imply a broad interfacial region and the associated density profiles for the interfacial region. Despite these limitations, the density profiles provide an overall view of the spatial organization in the RM. Qualitative insight into the water/surfactant headgroup interface can be obtained from the density profiles of the oxygen atom of water (O_w), the headgroup sulfur (S), and headgroup oxygen (O_s) atoms. Since Na^+ is associated with the surfactant headgroup, we calculate its density profile, as well. For information on the surfactant/hydrocarbon interface, we calculate the hydrocarbon density profile. All density profiles are presented in Figure 5.

First, we consider the profiles for the surfactant headgroup sites. For a reference spherical surface formed by S atoms, a delta function density profile is expected. As Figure 5 indicates, the S density profiles are broad, and this indicates a nonspherical arrangement of the surfactant at the water/headgroup interface, presumably due to fluctuations distorting the shape of the interface away from spherical symmetry. Associated with the same reference spherical surface formed by the S atoms, if headgroup O_s sites adopt identical orientations with respect to the radial direction, we would expect a delta function profile for O_s. Instead, analogous to the S density profile, we find a broad distribution of O_s sites, and this is compatible with the large number of O_s sites and their multiple orientations with respect to the S atom as well as a broad distribution of positions for the S atom.

Next, we consider the density profile for water at the interface with the surfactant headgroup, that is, the large-r region, which is most affected by confinement and high charge density effects. A simple reference system for studying the effect of confinement on density profiles is water within a hydrophobic cavity.[21] For this reference system, the density profile exhibits a small peak adjacent to the confining surface. In AOT RMs, the high charge density at the interface due to the headgroup should enhance the arrangement of water molecules beyond hydrophobic confinement. For the $w_0 = 2$ RM, we do see a sharp peak in the radial density profile, but it vanishes for the larger RMs. Since the O_s and S density profiles are the sharpest for $w_0 = 2$, the interfacial region has the most-well-defined arrangement of sites for the smallest RM, and this is lost or broadened due to the quasi-spherical fluctuating shape of the confining region formed by the surfactant headgroup.

Another change upon increasing the RM size is the broadening of the density profiles for S, O_s, and water in the interfacial region. This variation with w_0 is possibly due to the larger number of sites contributing to the density profile. An increase in RM size is also associated with a lowering of the interfacial free energy (and surface tension). Hence, it will be easier to distort the interface for the larger RM, and this manifests itself as enhanced interfacial flexibility. Quantitative tests for this and comparison with theoretical descriptions will be presented elsewhere.

Away from the interface in the interior of the RM, the density profile of water reaches a constant value consistent with bulk water for the $w_0 = 7.5$ RM. Deviation from this large-RM behavior starts becoming prominent by $w_0 = 4$ and is most significant for $w_0 = 2$. Due to the small size of $w_0 = 2$, the effect of confinement and charged groups at the interface is strong and persists inside the RM. This leads to a small peak in the interior, as well.

Since the AOT molecule contains a charged sulfonate headgroup and Na^+ counterion pair, we expect the Na^+ density profile to overlap with that for the AOT S atom and O_s atoms. This is, indeed, the case, and for all w_0, the position of the peak in the Na^+ density profile indicates proximity to the headgroup. The variation of its density profile with RM size is a consequence of the competition between breaking the headgroup ion-pair and solvation of Na^+ in water. As w_0 increases from 2.0 to 7.5, the density profile starts growing a small-r tail corresponding to an increase in the fraction of Na^+ ions solvated in the aqueous interior of the RM due to dissociation of the ion-pair. For $w_0 = 7.5$, there is a small region with width ~5 Å near the center of mass of the RM that does not contain any Na^+, and this should contain mostly bulklike water. For large-r, the extension of the Na^+ density profile beyond the O_w profile suggests these ions exist in the intersurfactant region and are coordinated to the surfactant carbonyl group.

Turning to the surfactant/hydrocarbon interface, the effect of varying w_0 on interfacial structure can be studied in terms of the hydrocarbon density profile. The small-r tail of the hydrocarbon density profile corresponds to the interfacial region and appears to overlap with the O_w density profile. This slight overlap in the density profile does not indicate the presence of a water/hydrocarbon interface. Instead, it suggests that shape fluctuations of the RM allow a few hydrocarbon molecules to enter the region between surfactant molecules. An increase in w_0 is associated with a more diffuse small-r region, and this is

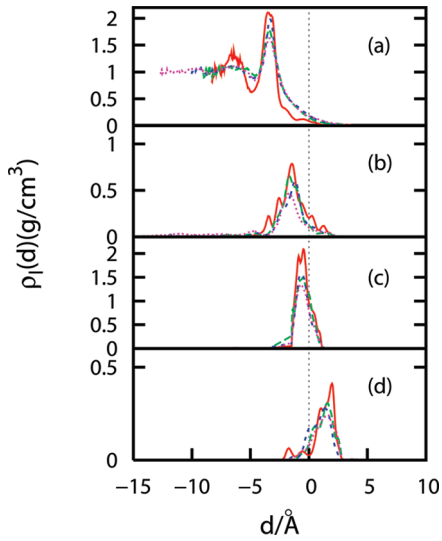

Figure 6. Intrinsic density profile, $\rho_I(d)$, for (a) O_w, (b) Na^+, (c) O_s, and (d) O_c for the proximal carbonyl oxygen in the $w_0 = 2$ (solid/red line), 4 (large dashes/green), 5.1 (small dashes/blue), and 7.5 (dots/pink) RM.

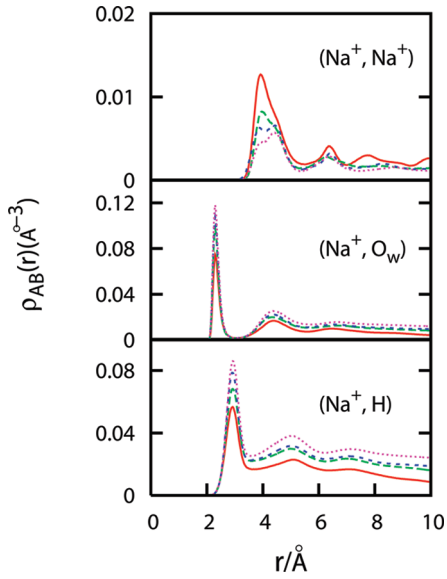

Figure 7. Pair density, $\rho_{AB}(r)$, for the (a) Na^+-O_w (b) Na^+-H, and (c) Na^+-Na^+ pairs in the $w_0 = 2$ (solid/red line), 4 (large dashes/green), 5.1 (small dashes/blue), and 7.5 (dots/pink) RM.

possibly the effect of lower surface tension for the larger RMs. As r increases, the hydrocarbon density increases, and a peak can be identified for the smallest RM. For the larger RMs, this peak vanishes, possibly due to larger-amplitude fluctuations at the interface. At large r, the hydrocarbon density reaches bulk values of 0.70 g/cm^3, a few hydrocarbon molecular diameters from the aqueous phase.

B. Intrinsic Density Profile. Our objective here is to study the truly interfacial structure by removing the effects broadening due to shape fluctuations. Since the S atoms for all AOT molecules forming the RM are unevenly distributed with respect to the center of mass, averaging beyond $-r_m$ is poor, and we truncate the intrinsic density profiles at $d = -r_m$. The density profiles with respect to the locally spherical intrinsic surface for all RM sizes are presented in Figure 6 and reveal interfacial structure that is fairly similar for all w_0.

The intrinsic density profiles for water are presented in Figure 6a and reveal a very structured profile unlike the radial density profile. The prominent first peak at $d \sim -3.5$ Å followed by a weaker peak at $d \sim -6.5$ Å is similar to the intrinsic density profile of water observed in interfaces with a hydrocarbon[39] or a lipid bilayer[43] and in a phosphate fluorosurfactant[44] RM. The first peak is most prominent for $w_0 = 2$ and indicates the presence of a rigid interface with glassy water. An increase in w_0 is associated with the decrease in peak height and an increase in the peak width, both of which imply a more fluid interfacial region for the larger RM. In the RM interior, the intrinsic density reaches the bulklike value of $\sim$1 g/cm^3 for $w_0 = 7.5$. All fluctuations with respect to this limiting density vanish within 10 Å from the intrinsic surface, and this is common to several commonly studied interfaces.[39,43] A small fraction of water molecules occupy the intersurfactant region and exist outside the intrinsic surface, as revealed by the finite but small density at $d > 0$.

Turning to Na^+, the intrinsic density profile in Figure 6b is of an almost Gaussian shape. It is most structured for $w_0 = 2$ but broadens as w_0 increases. The presence of structure in the $w_0 = 2$ intrinsic profile indicates a rigid interfacial region, since a flexible interface would broaden the profile due to diffusion of Na^+. The peak position is exterior to the first peak of O_w, does not change significantly with RM size, and indicates the existence of a well-defined position of Na^+ in the counterion−sulfonate pair. As the RM size increases, the density in the interior of the RM increases as a consequence of enhanced dissociation of these counterion−headgroup pairs.[21] A finite population of Na^+ ions exists in the intersurfactant region and outside, where it must be coordinated with the carbonyl group.

The O_s atoms occupy a well-defined region normal to the intrinsic surface, as evident from the narrow, intrinsic profile in Figure 6c. The peak position of $d \sim -1.2$ Å is on the order of the distance of the headgroup sulfur−oxygen bond projected along the direction from the sulfur atom to the center of mass of the oxygen atoms. The $w_0 = 2$ RM has the largest density, and this corresponds to a rigid interface as indicated by the Na^+ and O_w intrinsic profiles. As the RM size increases, the peak height decreases with respect to $w_0 = 2$, but it is does not change significantly beyond $w_0 = 4$. The large-d edge of the profile is broader due to availability of more space for orienting the headgroup at the interface.

Finally, we present the intrinsic profile for the proximal carbonyl oxygen (O_c) in Figure 6d. The radial density profile for O_c was not presented in the previous section. Although each AOT has two carbonyl groups (Figure 1), we do not observe a significant difference in their intrinsic profiles and present the results for the proximal carbonyl oxygen only. Since the solvent preferentially solvates the surfactant hydrophobic tails, the large-d region of the profile sharply cuts off at $d \sim 2.5$ Å, and this is the opposite of the O_s intrinsic profile. The overlap in density profiles of O_w, O_s, and O_c is due to a combination of aqueous solvation of the carbonyl group and AOT conformational flexibility.

IV. Pair Densities

Although the radial and intrinsic density profiles provide information on the overall arrangement of molecules in the RM, the pair structure complements the information on intramolecular arrangements. As done in previous work,[21] for a given pair of species A and B, we defined the pair density $\rho_{AB}(r)$ such that $4\pi\ \rho_{AB}(r)\ r^2\ dr$ is the average number of species B that are in the distance range between r and $r + dr$ away from species A.

We present the Na^+-Na^+ pair densities in Figure 7, and the corresponding number of ions in the first coordination shell are

TABLE 2: Number of First Coordination Shell Neighbors of Species B around a Central Species A for the Atomic Pair A−B

RM	Na^+-O_w	Na^+-H	Na^+-Na^+	O_s-O_w	O_s-H	O_s-Na^+	O_c-O_w	O_c-H	O_c-Na^+	S−S	O_s-O_s
RM2	1.53	4.42	3.00	2.62	0.72	1.55	1.03	0.26	0.75	3.99	1.53
RM4a	1.85	5.25	2.11	3.17	1.09	1.33	0.93	0.26	0.76	3.32	1.14
RM5.1	2.08	5.66	1.99	3.41	1.13	1.23	1.50	0.33	0.76	2.93	0.86
RM7.5	2.26	6.13	1.63	3.43	1.20	1.18	1.63	0.39	0.70	2.74	0.87

reported in Table 2. For $w_0 = 2$, each Na^+ is tricoordinated in agreement with previous simulations of Faeder and Ladanyi,[23] where a single-site representation for the sulfonate headgroup was utilized. Due to shape fluctuations of the RM, it is not easy to identify the local coordination by visual inspection alone. Upon varying RM size, the broad first peak of the $w_0 = 2$ RM splits into an inner peak whose height decreases with an increase in w_0 and an outer peak whose height increases with w_0. Clearly, an increase in the RM size leads to a larger inter-Na^+ separation, which allows more molecules to coordinate with the counterion, and this is in agreement with ^{23} Na NMR experiments.[55,56]

Solvation of Na^+ in water is studied in terms of the pair densities presented in Figure 7. Interaction of Na^+ with water is governed by ion−dipole interactions, and we expect O_w to be closer to the ion than the hydrogen atom of water. From Figure 7, we note that this is, indeed, the case for all RM sizes. An increase in w_0 causes an increase in the magnitudes of the Na^+-O_w and Na^+-H pair densities, especially the first peak. Thus, more water molecules are coordinated to each Na^+ as the RM size increases, and this is associated with the increase in the inter-Na^+ distance. The number of O_w's in the first coordination shell of each Na^+ in the $w_0 = 2$ RM is 1.53 (Table 2). This can be interpreted as the presence of pairs of Na^+ bridged by one water molecule.

Experiments probing the sulfonate stretching modes[49−54] provide information on the local environment. We present our results for the O_s−water and O_s-Na^+ pair densities in Figure 8 and the corresponding first shell coordination numbers in Table 2. Since O_s forms hydrogen bonds with the water molecules, we expect the first peak in the O_s-H pair density function to be closer to O_s than that for the O_s-O_w pair density. Our data supports this picture. The number of H and O_w atoms in the first coordination shell increases with RM size. Along with this increase in headgroup hydrogen bonding, the coordination number of Na^+ decreases with RM size. These two observations confirm dissociation of the headgroup−counterion pair, which is associated with an increase in solvation of both O_s and Na^+ sites. The strong first peak in the O_s-Na^+ pair density for $w_0 = 2$ contains 1.55 sodium ions, which corresponds to a picture of three sodium ions shared among pairs of neighboring O_s sites. Placed together with the tricoordinated structure of Na^+, these observations support a pseudolattice structure for the sodium−sulfonate pair, as inferred from calorimetric data by Shen et al.[57]

In Section III B, the intrinsic density profiles for O_c (Figure 6) indicated a region shared with water and Na^+. This raises the possibility of solvation of O_c by these two molecular species; this should modify the AOT carbonyl vibrational frequencies. The relevant pair densities for O_c are presented in Figure 9. Both O_c-O_w and O_c-H pair densities show a first peak that broadens with increasing w_0. The number of H atoms in the first coordination shell increases only slightly, whereas the number of O_w atoms increases more. These changes indicate the availability of more water molecules in the intersurfactant region as the RM size increases.

As evident from the density profiles, Na^+ ions exist in the region occupied by the sulfonate headgroup and carbonyl oxygen atoms. This suggests possible Na^+-O_c coordination. The well-defined first peak in the Na^+-O_c pair density implies that favorable interactions with Na^+ may be an additional driving force for solvation of the carbonyl group in the water pool. The local coordination number of 0.75 for all RM sizes indicates that Na^+ may be shared with the O_s atom of neighboring surfactant headgroups.

Next, we present the pair structure of the surfactant headgroup by constructing the pair densities for S−S, S−O_s (O_s on a

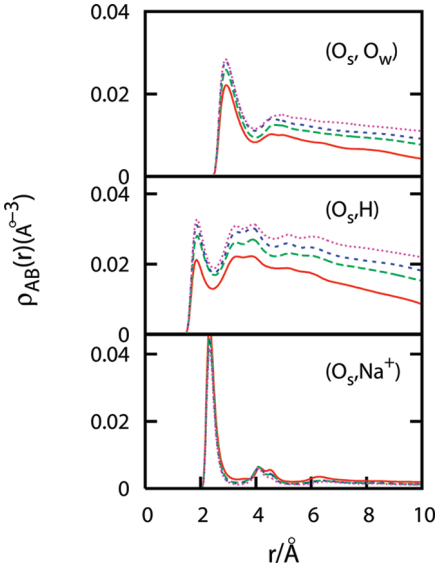

Figure 8. Pair density, $\rho_{AB}(r)$, for the (a) O_s-O_w (b) O_s-H, and (c) O_s-Na^+ pairs in the $w_0 = 2$ (solid/red line), 4 (large dashes/green), 5.1 (small dashes/blue), and 7.5 (dots pink) RM.

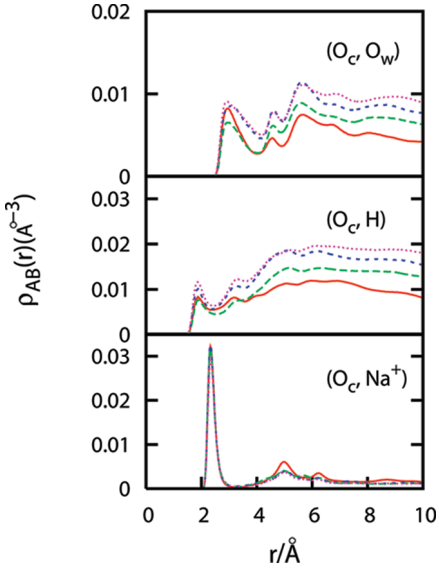

Figure 9. Pair density, $\rho_{AB}(r)$, for the (a) O_c-O_w (b) O_c-H and (c) O_c-Na^+ pairs in the $w_0 = 2$ (solid/red line), 4 (large dashes/green), 5.1 (small dashes/blue), and 7.5 (dots/pink) RM.

neighboring sulfonate), and the O_s-O_s (the oxygen atoms on distinct sulfonates) pairs. From Figure 10, the typical S−S pair separation is ∼5.2 Å. Increasing the RM size broadens the peak width and shifts the peak position to large r. Thus, more water and Na^+ are included between neighboring headgroups with an increase in w_0. The number of S atoms in the first solvation shell for $w_0 = 2$ of 4 corresponds to four coordinated sulfonate groups. Using a single site representation for the sulfonate group, Faeder and Ladanyi[23] found the same coordination. An increase in the surface area with w_0 reduces the geometrical confinement, thereby allowing for a more relaxed network of S atoms at the water/surfactant headgroup interface.

The O_s-O_s pair density shows a well-defined first peak at ∼2.75 Å, followed by a broad secondary peak of similar height at ∼4.25 Å. The presence of 1.53 neighbors in the first coordination shell of O_s follows the same trend of sharing three neighboring atoms in the pair densities for O_s-Na^+ (1.56) and O_w-Na^+ (1.53) and suggests a lattice structure for $w_0 = 2$. For the larger RMs, this pseudolattice structure breaks down, and the number of O_s atoms in the first peak decreases to 0.87 for $w_0 = 7.5$. Finally, we note that the pair densities for $S-O_s$ are broad and have multiple peaks. The first coordination shell corresponds to the region $r < 4.8$ Å independent of w_0. The broad first peak for $w_0 = 2$ shifts to larger r and becomes narrower for the larger RM. Associated with this, the number of atoms in the first coordination shell decreases, a feature expected from the expected breakdown of the pseudolattice structure for the large RMs.

V. Pair Orientation in the First Coordination Shell

In the previous section, pair structure was studied in terms of the pair densities. A more detailed description of RM structure requires information on triplet and higher-order correlations. We avoid the extensive interpretation of data inherent to higher-order structure. Instead, we focus our attention on complementing the pair densities for the A−B and B−C pairs with information on the mutual orientation of the pairs of sites when both one of the sites, A or C, lies within the first coordination shell of B and the second site, C or A, is covalently bonded to B or a molecular vector associated with B (such as the dipole vector of water). The information generated by these triplets sheds light on the relative organization of a site with respect to a molecular vector. For a given triplet ABC, the fraction of all triplets, $P[\cos(\theta)]$, that contain an angle of θ at site B is calculated. For reference, if all triplet orientations are equally likely, $P[\cos(\theta)]$ is a constant.

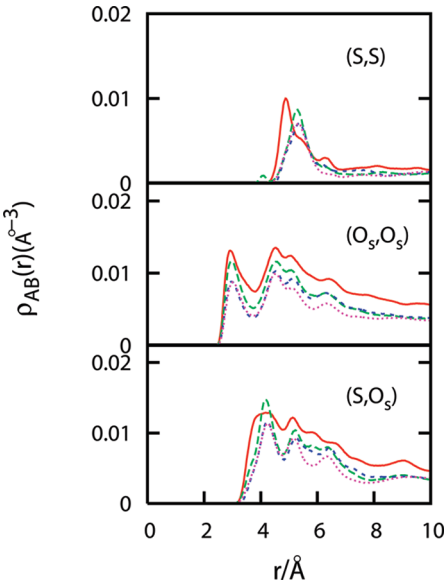

Figure 10. Pair density, $\rho_{AB}(r)$, for the (a) S−S (b) O_s-O_s, and (c) $S-O_s$ pairs in the $w_0 = 2$ (solid/red line), 4 (large dashes/green), 5.1 (small dashes/blue), and 7.5 (dots/pink) RM.

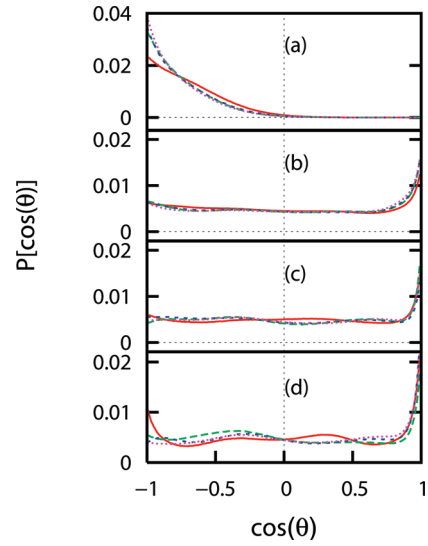

Figure 11. Distribution of orientations, $P[\cos(\theta)]$, between the water dipole vector and the (a) O_w-Na^+ (b) O_w-O_s, (c) O_w-O_c vector for the proximal carbonyl and (d) the O_w-O_c vector for the distal carbonyl for the $w_0 = 2$ (solid/red line), 4 (large dashes/green), 5.1 (small dashes/blue), and 7.5 (dots/pink) RM.

Because water molecules are associated with Na^+, O_s, and the two O_c atoms on each AOT ion, we present the distribution of orientations of the dipole moment vector of water with respect to the O_w-Na^+ vector in Figure 11a. The ion−dipole interaction between the water and Na^+ leads to O_w being closer to Na^+ than H, and the water dipole vector is expected to be oriented primarily along the O_w-Na^+ direction away from Na^+. For all RMs studied, this is the case, and most water dipole vectors point away from Na^+. Varying the RM size increases the number of water molecules adopting this preferred orientation. The broader distribution of orientations for $w_0 = 2$ is related to its small size, which leads to stronger interaction with headgroup sites organized in a pseudolattice.

The O_s and the two O_c atoms of the surfactant molecule act as hydrogen bond acceptors. For an ensemble of linear hydrogen bonds (triplet with bridging hydrogen atom), $P[\cos(\theta)]$ will be a delta function centered at $\cos(\theta) = 1$ and at $\cos(\theta) = -0.58$ (corresponding to the $H-O_w-H$ bond angle of ∼109° for SPC/E water). Deviations from these reference triplet orientations correspond to local fluctuations as well as preferential arrangement due to the presence of charged and crowded interfacial environment in the RM. Hence, it is useful to study the orientation of O_w-H with respect to the O_w-O_s and O_w-O_c vectors. We present the distribution of orientations for the $H-O_w-O_s$ pairs in Figure 11b. The distribution for all w_0's shows two prominent orientations: (1) maximum at $\cos(\theta) = 1$ corresponding to a linear O_w-H-O_s triplet and (2) maximum at $\cos(\theta) = -1$ corresponding to a linear $H-O_w-O_s$ triplet. The first orientation is typical of linear hydrogen bonds and is broadest for $w_0 = 2$, possibly due to the availability of other triplet orientations. A consequence of the geometrically constrained environment is the presence of bent O_s−hydrogen bonds, which are associated with the linear $H-O_w-O_s$ preferred arrangement. These bent hydrogen bonds are possibly indicative of hydrogen atoms bridging multiple O_s sites.

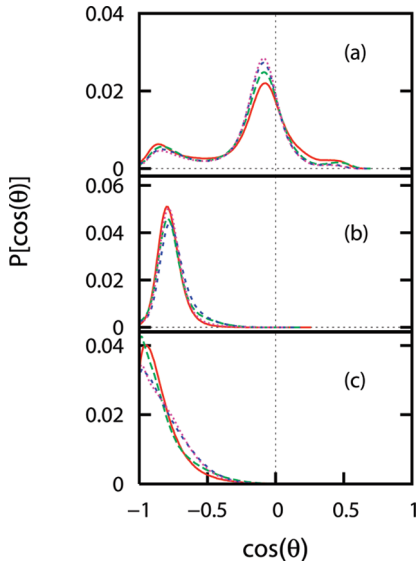

Figure 12. Distribution of orientations, $P[\cos(\theta)]$, between the (a) Na^+-O_s and O_s-S vectors, (b) Na^+-O_c and O_c-C vector for the proximal carbonyl, and (c) the Na^+-O_c and O_c-C vector for the distal carbonyl for the $w_0 = 2$ (solid/red line), 4 (large dashes/green), 5.1 (small dashes/blue), and 7.5 (dots/pink) RM.

Turning to the carbonyl oxygen atoms, the distribution of triplet orientations is presented in Figure 11c and d for the proximal and distal carbonyl oxygen atoms, respectively. Both distributions contain a narrow peak at $\cos(\theta) = 1$ corresponding to a linear hydrogen bond with the carbonyl oxygen. This peak is narrower than that seen for hydrogen bonds with the sulfonate and indicates a high degree of directionality for the hydrogen bond of water with the carbonyl oxygen. The proximal carbonyl does not exhibit any other significant orientational preference. The triplet orientation distribution for the distal carbonyl, on the other hand, has additional structure corresponding to peaks at $\theta \sim 114°$ for all w_0's and indicates a slightly bent O_w-H-O_c bond. The $w_0 = 2$ RM exhibits additional peaks corresponding to $\theta \sim 180°$ and 70°, which reflect additional coordination of the water molecule to the ester oxygen due to the extreme confinement in the RM. Clearly, the two O_c's are not equivalent, and this should be observed in the carbonyl stretch frequencies.

Noting that the density profiles for Na^+, O_s, and O_c overlap and the pair densities indicate a small population of Na^+ in the first coordination of O_c, we present the triplet orientation distribution for Na^+ with respect to the O_s-S and O_c-C vectors in Figure 12. From Figure 12a, we note that the Na^+ ion is oriented primarily orthogonal to the O_s-S vector, which could correspond to the Na^+ ion coordinated with the three O_s of a headgroup, or it might indicate a bridging role between headgroups. A secondary preferred orientation at $\theta \sim 26°$ corresponds to a slightly bent Na^+-O_s-S triplet.

A small fraction of all Na^+ is associated with the carbonyl oxygen. The local geometry involved with this pair of sites can be quantified in terms of the angle between the Na^+-O_c and O_c-C vectors (where C is the carbonyl carbon). Its distribution is presented in Figure 12b and c. The dominant arrangement corresponds to a bent Na^+-O_c-C orientation with an angle of ~38° and ~5° for the proximal and distal carbonyl groups, respectively. The linear arrangement for the distal O_c suggests coordination with Na^+ that bridges multiple O_s sites. The bent arrangement possibly arises due to the two ester oxygens being coordinated to water molecules as well as to Na^+. The size of the RM has a weak effect on the local arrangement of the sodium ion around the proximal O_c. For the distal O_c, an increase in w_0 is associated with an increase in the fraction of linear triplets, although the corresponding broadening of the distribution indicates the availability of multiple orientations.

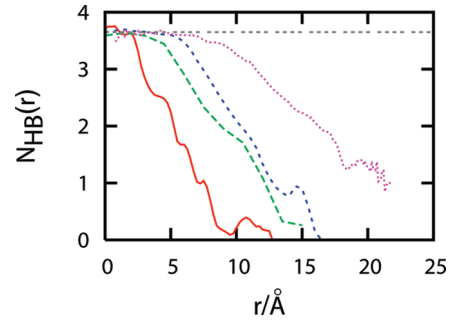

Figure 13. Radial variation of the number of hydrogen bonds, $N_{HB}(r)$, for the (a) $w_0 = 2$ (solid/red line), (b) 4 (large dashes/green), (c) 5.1 (small dashes/blue), and (d) 7.5 (dots/pink) RMs.

VI. Hydrogen Bond Distribution of Water

The water molecules in the RM are part of a hydrogen bonded network that is perturbed with respect to the bulk due to the presence of the surfactant headgroup and counterions. These perturbations lead to experimentally observed variations of OH/OD frequencies, which indicate reduced hydrogen bonding in the RM.[47] We quantify the local hydrogen bond network in terms of the number of hydrogen bonds made by a water molecule with the neighboring water molecules only. For this purpose, a pair of water molecules is considered hydrogen bonded if the O−O distance is smaller than 3.5 Å and the O−O−H angle is smaller than $\pi/6$.[73] This criterion for hydrogen bond identification is suitable for bulk water and may have to be modified for water adjacent to an ion.[74] However, we will retain the bulk water hydrogen bond definition for now. The hydrogen bonded state of an instantaneous configuration is characterized by the variable $h_{i,j}(t)$ which takes a value of 1 or 0 at time t, depending on whether the molecules i and j are hydrogen bonded or not. A key structural characteristic of the hydrogen bonded network is the average number of hydrogen bonds per molecule, $N_{HB} = \langle h_{i,j} \rangle$. We present its radial variation, $N_{HB}(r)$, in Figure 13. For bulk water, we estimate the number of hydrogen bonds at 3.6, and this serves as a reference for the deviation of the local hydrogen bond network from bulk.

For $w_0 = 2$, $N_{HB}(r)$ exhibits a fluctuating decay from a value of 3.7 at $r = 0$ Å to 0 at $r = 12.5$ Å. These fluctuations are mostly a consequence of the enhanced density of water adjacent to the intrinsic S surface coupled with the pseudolattice arrangement of the interfacial region. An increase in the RM size is associated with a small r plateau in $N_{HB}(r)$, followed by a smoother decay of $N_{HB}(r)$. The plateau value is almost independent of the RM size, and the radial range for which this plateau exists increases from about 5 Å for $w_0 = 4$ to 7.5 Å for $w_0 = 7.5$. Only the $w_0 = 7.5$ system has a bulklike interior. For water molecules in the intersurfactant region, the number of hydrogen bonds decreases to zero up to $w_0 = 5.1$, but for $w_0 = 7.5$, one hydrogen bond exists in the outermost region and possibly indicates a water molecule simultaneously hydrogen bonded to the water droplet and carbonyl oxygen.

VII. Discussion

In this work, molecular dynamics simulations were performed to study the size-dependent structure of AOT reverse micelles. The spherically symmetric radial and the intrinsic density

profiles were constructed to gain insight into the overall arrangement of molecules at the water/surfactant headgroup interface and interior to the RM. The organization of molecular pairs was studied in terms of the pair distribution functions and the pair orientation distributions in the first coordination shell. Finally, the multimolecular organization of water molecules in the hydrogen bonded network was probed by calculating the number of hydrogen bonds at different radial locations in the RM.

A complete picture of interfacial structure at the water/surfactant headgroup interface must account for the organization of the surfactant headgroup, sodium ions, and water molecules at the interface. For the smallest RM studied, our data supports a picture where each sulfonate group has four neighboring sulfonates in the first coordination shell. Within the sulfonate lattice, the sulfonate oxygens are organized such that each oxygen atom has three neighboring sulfonate oxygen atoms contributed by the adjacent headgroups. A sodium ion is shared between pairs of sulfonate oxygen atoms on distinct headgroups, and this arrangement ensures that each sodium ion has exactly three neighboring sodium ions. The observed interfacial arrangement is no doubt a consequence of the local curvature that governs the local packing of molecules.

At infinite dilution, the sodium ion is coordinated to up to six water molecules.[75] For the $w_0 = 2$ RM, we find that each sodium ion is coordinated to three water oxygens, but each water molecule is shared between two sodium ions. Furthermore, each sodium ion is shared with three sulfonate oxygens and this presumably completes the hexa coordination at the interface analogous to that of the sodium ion at infinite dilution. Since we start the simulation with a random distribution of sodium ions, it would appear that this organization of sodium ions corresponds to at least a metastable equilibrium, if not an equilibrium, configuration. The presence of a pseudolattice for the smallest RM has been suggested before,[57] and our results support this interfacial arrangement.

An increase in the RM size leads to additional flexibility of the interface due to disruption of the pseudolattice. Ion pairs dissociate, and aqueous solvation of the sodium ions as well as the sulfonate oxygens sets in. Interpretation of the vibrational spectrum of sulfonate symmetric and asymmetric stretches as well as ^{23} Na NMR lead to a scenario for interfacial structure in which the water molecules act as bridges between the sodium ion and the sulfonate oxygen.[54] Although this arrangement of molecules differs from the one inferred from our analysis of simulation data for the $w_0 = 2$, perhaps it represents an equilibrium local structure for the larger RMs in which the combination of ion−headgroup pair dissociation and aqueous solvation of the headgroup may support its existence. In fact, the number of hydrogen atoms coordinated to the sulfonate oxygen increases to more than one as RM size increases, supporting the view that the headgroup is solvated.

Does the presence of the pseudolattice structure for the ion−headgroup pair imply the absence of water molecules exterior to the headgroup sulfur atom? Our analysis of the intrinsic density profile suggests this is not the case, since a small fraction of water molecules do exist exterior to the intrinsic surface. Thus, water molecules can be hydrogen bonded to the sulfonate group, the ester carbonyl, sodium ions, and to other water molecules, just as inferred from curve-fitting of the O−H stretching band observed in FTIR[12,13,17] experiments.

As RM size increases, more water molecules are present in an environment far from the interface. Are the interior-most water molecules bulklike? From the analysis of density (which should approach values of 0.997 g/cm^3 for water) and the number of hydrogen bonds (which should reach bulklike values of 3.6), we infer the absence of bulklike water in the interior of the RM for $w_0 \leq 5.1$. Since we did not simulate the $w_0 = 6$ RM, it is unclear if it has a bulklike interior. However, the $w_0 = 7.5$ RM clearly has a small bulklike region, which might persist for slightly smaller RMs. Only for RM sizes close to $w_0 = 7.5$ can we expect the aqueous interior to contain a region with structural characteristics consistent with bulk water. These observations differ slightly from the previous studies of Faeder and Ladanyi[21] for a reduced model, since the presence of shape fluctuations perturbs the water network toward the interior of the RM. The intrinsic density profile for water contains a region 10 Å from the headgroup sulfur atoms that is bulklike. Thus, it is reasonable to consider these molecules as belonging to the core region in the core−shell model. The presence of a bulklike core for RM radius comparable to and larger than $w_0 = 7.5$ has important implications for the solvation of biomolecules in RMs.[15,76]

As indicated by the intrinsic density profiles, the interfacial region within 10 Å from the headgroup sulfur atoms contains two well-defined peaks. The first peak corresponds to water molecules interacting directly with the headgroup and represents an outermost shell region. Water molecules contributing to the second peak bridge the outermost shell to those in the inner core. In terms of the core−shell model, the structure of the shell region should therefore be reinterpreted as comprising at least two subshell regions identified with the two peaks in the intrinsic density profile for water. Starting with a dry RM (no water) and adding water molecules to the interior, water molecules populate the outermost shell; followed by the inner shell; and finally, the core. The size of the RM determines the distance at which the intrinsic density profile should be truncated. In view of these observations, the traditional view of a core−shell structure should be revised.

In concluding, we hope this work will be a step toward a quantitative picture of RM structure and help in the interpretation of experimental data. Subsequent work will address single molecular relaxation, hydrogen bond dynamics, and the thermodynamic as well as hydrodynamic description of interfacial fluctuations. Given the insight into local structure, it would be useful to relate the changes with RM size to the vibrational spectrum for the OH/OD bond,[77] ester carbonyl, and vibrational modes of the sulfonate group.

Acknowledgment. This work was supported by DOE Grant DE-FG03-0ZER15376 and by NSF Grant CHE 0608640.

Supporting Information Available: The molecular and force field parameters used in the simulation are presented as Supporting Information. This material is available free of charge via the Internet at http://pubs.acs.org.

References and Notes

(1) Luisi, P. L.; Straub, B. E. Eds. *Reverse Micelles*; Plenum: New York, 1984.

(2) Langevin, D. *Acc. Chem. Res.* **1988**, *21*, 255.

(3) Gelbart, W. M.; Ben-Shaul, A.; Roux, D. Eds. *Micelles, Membranes, Microemulsions, and Monolayers*; Springer: Berlin, 1994.

(4) De, T. K.; Maitra, A. *Adv. Colloid Interface Sci.* **1995**, *59*, 95.

(5) Luisi, P. L.; Giomini, M.; Pileni, M. P.; Robinsion, B. H. *Biochim. Biophys. Acta* **1988**, *947*, 209.

(6) Pileni, M. P. *Ber. Bunsenges. Phys. Chem.* **1997**, *101*, 1578.

(7) Chang, G. G.; Huang, T. M.; Hung, H. C. *Proc. Natl. Sci. Counc. Repub. China B* **2000**, *24*, 89.

(8) Pohorille, A.; Deamer, D. W. *Trends Biotechnol.* **2002**, *20*, 123.

(9) Swami, A.; Espinosa, G.; Guillot, S.; Raspaud, E.; Boue, F.; Langevin, D. *Langmuir* **2008**, *24*, 11828.
(10) Venables, D. S.; Huang, K.; Schmuttenmaer, C. A. *J. Phys. Chem. B* **2001**, *105*, 9132.
(11) Boyd, J. E.; Briskman, A.; Sayes, C. M.; Mittleman, D.; Colvin, V. *J. Phys. Chem. B* **2002**, *106*, 6346.
(12) Piletic, I. R.; Moilanen, D. E.; Spry, D. B.; Levinger, N. E.; Fayer, M. D. *J. Phys. Chem. A* **2006**, *110*, 4985.
(13) Dokter, A. M.; Woutersen, S.; Bakker, H. J. *Proc. Natl. Acad. Sci. U.S.A.* **2006**, *103*, 15355.
(14) Cringus, D.; Bakulin, A.; Lindner, J.; Vöhringer, P.; Pshenichnikov, M. S.; Wiersma, D. A. *J. Phys. Chem. B* **2007**, *111*, 14193.
(15) Johnston, K. P.; Harrison, K. L.; Clarke, M. J.; Howdle, S. M.; Heitz, M. P.; Bright, F. V.; Carlier, C.; Randolph, T. W. *Science* **1996**, *271*, 624.
(16) Rosenfeld, D. E.; Schmuttenmaer, C. A. *J. Phys. Chem. B* **2006**, *110*, 14304.
(17) Moilanen, D. E.; Levinger, N. E.; Spry, D. B.; Fayer, M. D. *J. Am. Chem. Soc.* **2007**, *129*, 14311.
(18) Levinger, N. E. *Science* **2002**, *298*, 1722.
(19) Nave, S.; Eastoe, J.; Heenan, R. K.; Steytler, D.; Grillo, I. *Langmuir* **2000**, *16*, 8741.
(20) Alaimo, M. H.; Kumosinski, T. F. *Langmuir* **1997**, *13*, 2007.
(21) Faeder, J.; Ladanyi, B. M. *J. Phys. Chem. B* **2000**, *104*, 1033.
(22) Faeder, J.; Ladanyi, B. M. *J. Phys. Chem. B* **2001**, *105*, 11148.
(23) Faeder, J.; Albert, M. V.; Ladanyi, B. M. *Langmuir* **2003**, *19*, 2514.
(24) Faeder, J.; Ladanyi, B. M. *J. Phys. Chem. B* **2005**, *109*, 6732.
(25) Abel, S.; Sterpone, F.; Bandyopadhyay, S.; Marchi, M. *J. Phys. Chem. B* **2004**, *108*, 19458.
(26) Gardner, A.; Vasquez, V. R.; Clifton, A.; Graeve, O. A. *Fluid. Phase Equilib.* **2007**, *262*, 264.
(27) Mudzhikova, G. V.; Brodskaya, E. N. *Colloid J.* **2006**, *68*, 729.
(28) Mudzhikova, G. V.; Brodskaya, E. N. *Colloid J.* **2006**, *68*, 738.
(29) Allen, R.; Bandyopadhyay, S.; Klein, M. L. *Langmuir* **2000**, *16*, 10547.
(30) Senapati, S.; Keiper, J. S.; DeSimore, J. M.; Wignall, G. D.; Melnichenko, Y. B.; Frielinghaus, H.; Berkowitz, M. L. *Langmuir* **2002**, *18*, 7371.
(31) Watanabe, K.; Ferrario, M.; Klein, M. L. *J. Phys. Chem.* **1988**, *92*, 819.
(32) Watanabe, K.; Klein, M. L. *J. Phys. Chem.* **1989**, *93*, 6897.
(33) MacKerell, A. *J. Phys. Chem.* **1995**, *99*, 1846.
(34) Salaniwal, S.; Cui, S. T.; Cochran, H. D.; Cummings, P. T. *Ind. Eng. Chem. Res.* **2000**, *39*, 4543.
(35) Salaniwal, S.; Cui, S. T.; Cochran, H. D.; Cummings, P. T. *Langmuir* **2001**, *17*, 1773.
(36) Buff, F. P.; Lovett, R. A.; Stillinger, F. H. *Phys. Rev. Lett.* **1965**, *15*, 621.
(37) Henderson, J. R.; Schofield, P. *Proc. R. Soc. London A* **1982**, *380*, 211.
(38) Chacon, E.; Tarazona, P. *Phys. Rev. Lett.* **2003**, *91*, 166103.
(39) Chowdhary, J.; Ladanyi, B. M. *J. Phys. Chem. B* **2006**, *110*, 15442.
(40) Chowdhary, J.; Ladanyi, B. M. *J. Phys. Chem. B* **2008**, *112*, 6259.
(41) Chowdhary, J.; Ladanyi, B. M. *Phys. Rev. E* **2008**, *77*, 031609.
(42) Bresme, F.; Chacon, E.; Tarazona, P.; Tay, K. *Phys. Rev. Lett.* **2008**, *101*, 056102.
(43) Pandit, S. A.; Bostick, D.; Berkowitz, M. L. *J. Chem. Phys.* **2003**, *119*, 2199.
(44) Senapati, S.; Berkowitz, M. L. *J. Phys. Chem. B* **2003**, *107*, 12906.
(45) Senapati, S.; Berkowitz, M. L. *J. Chem. Phys.* **2003**, *118*, 1937.
(46) Senapati, S.; Berkowitz, M. L. *J. Phys. Chem. A* **2004**, *108*, 9768.
(47) Onori, G.; Santucci, A. *J. Phys. Chem.* **1993**, *97*, 5430.
(48) D'Angelo, M.; Onori, G.; Santucci, A. *J. Phys. Chem.* **1994**, *98*, 3189.
(49) Deak, J. C.; Pang, Y. S.; Sechler, T. D.; Wang, Z. H.; Dlott, D. D. *Science* **2004**, *306*, 473.
(50) MacDonald, H.; Bedwell, B.; Gulari, E. *Langmuir* **1986**, *2*, 704.
(51) Jain, T. K.; Varshney, M.; Maitra, A. *J. Phys. Chem.* **1989**, *93*, 7409.
(52) Moran, P. D.; Bowmaker, G. A.; Cooney, R. P.; Bartlett, J. R.; Woolfrey, J. L. *Langmuir* **1995**, *11*, 738.
(53) Gonzalez-Blanco, C.; Rodriguez, L. J.; Velazquez, M. M. *Langmuir* **1997**, *13*, 1938.
(54) Li, Q.; Weng, S. F.; Wu, J.; Zhou, N. F. *J. Phys. Chem. B* **1998**, *102*, 3168.
(55) Wong, M.; Thomas, J. K.; Nowak, T. *J. Am. Chem. Soc.* **1977**, *99*, 4730.
(56) Kenez, P. H.; Carlstrom, G.; Furo, I.; Halle, B. *J. Phys. Chem.* **1992**, *96*, 9524.
(57) Shen, X. H.; Gao, H. C.; Wang, X. Y. *Phys. Chem. Chem. Phys.* **1999**, *1*, 463.
(58) Wootton, A.; Picavez, F.; Harrowell, P. *AIP Conf. Proc.* **2008**, *982*, 289.
(59) Berendsen, H. J. C.; Grigera, J. R.; Straatsma, T. P. *J. Phys. Chem.* **1987**, *91*, 6269.
(60) Schweighofer, K. J.; Essmann, U.; Berkowitz, M. L. *J. Phys. Chem. B* **1997**, *101*, 3793.
(61) Martin, M. G.; Siepmann, J. I. *J. Phys. Chem. B* **1999**, *103*, 4508.
(62) Kamath, G.; Robinson, J.; Potoff, J. J. *Fluid Phase Equilib.* **2006**, *240*, 46.
(63) Schlenkrich, M.; Brickmann, J.; MacKerell, A. D.; Karplus, M. In *Biological Membranes: A Molecular Perspective from Computation and Experiment*; Birkhauser: Boston, 1996.
(64) Ewald, P. *Ann. Phys.* **1921**, *64*, 253.
(65) Allen, M. P.; Tildesley, D. J. *Computer Simulation of Liquids*; Oxford University Press: Oxford, 1989.
(66) Hummer, G.; Gronbech-Jensen, N.; Neumann, M. *J. Chem. Phys.* **1998**, *109*, 2791.
(67) Berendsen, H. J. C.; Postma, J. P. M.; van Gunsteren, W. F.; DiNola, A.; Haak, J. R. *J. Chem. Phys.* **1984**, *81*, 3684.
(68) Eicke, H.-F.; Rehak, J. *Helv. Chim. Acta* **1976**, *59*, 2883.
(69) Amararene, A.; Gindre, M.; Le Huerou, J.-Y.; Urbach, W.; Valdez, D.; Waks, M. *Phys. Rev. E* **2000**, *61*, 682.
(70) Zulauf, M.; Eicke, H.-F. *J. Phys. Chem.* **1979**, *83*, 480.
(71) Robinson, B. H.; Toprakcioglu, C.; Dore, J. C.; Chieux, P. *J. Chem. Soc., Faraday Trans. 1* **1984**, *80*, 13.
(72) Allen, R.; Bandyopadhyay, S.; Klein, M. L. *Langmuir* **2000**, *16*, 10547.
(73) Luzar, A.; Chandler, D. *Nature* **1996**, *379*, 55.
(74) Sharp, K. A.; Madan, B.; Manas, E.; Vanderkooi, J. M. *J. Chem. Phys.* **2001**, *114*, 1791.
(75) Koneshan, S.; Rasaiah, J. C.; Lynden-Bell, R. M.; Lee, S. H. *J. Phys. Chem. B* **1998**, *102*, 4193.
(76) Chaitanya, V. S. V.; Senapati, S. *J. Am. Chem. Soc.* **2008**, *130*, 1866.
(77) Pieniazek, P. A.; Lin, Y.-S.; Chowdhary, J.; Ladanyi, B. M.; Skinner, J. L. *J. Phys. Chem. B*, accepted for publication.

JP906915Q